RSC Advances




ROYAL SOCIETY OF CHEMISTRY

www.rsc.org/advances

RSC Advances

RSCPublishing

ARTICLE

# Sequential Radiation Chemical Reactions in Aqueous Bromide Solutions: Pulse Radiolysis Experiment and Spur Model Simulation

Cite this: DOI: 10.1039/x0xx00000x

Received 00th January 2012,
Accepted 00th January 2012

DOI: 10.1039/x0xx00000x

www.rsc.org/

S. Yamashita,[a] K. Iwamatsu,[b,c] Y. Maehashi,[b] M. Taguchi,[c] K. Hata,[d] Y. Muroya[e] and Y. Katsumura[a,b],

Pulse radiolysis experiments were carried out to observe transient absorptions of reaction intermediates produced in $N_2O$- and Ar-saturated aqueous solutions containing 0.9-900 mM NaBr. The most important species among the reaction intermediates are $BrOH^{\bullet-}$ and $Br_2^{\bullet-}$, which commonly have absorption peaks around 360 nm. Experimental results were compared to results of simulation based on spur diffusion model. Each of complicated sequential radiation chemical reactions was carefully considered with optimizing its rate constant within a range of reported values including experimental uncertainty. All the experimental results covering a wide variety of conditions were able to be universally reproduced by the simulation with assuming a not yet reported reaction, $BrOH^{\bullet-} + BrOH^{\bullet-} \rightarrow Br_2 + 2OH^-$, with rate constant of $3.8\times10^9$ $M^{-1}s^{-1}$, which is significant only within 10 μs for rather high bromide concentration (> 10 mM). Primary G values, which are yields after sufficient diffusions from spur to perimeter region during 100 ns, of major water decomposition products as well as of the reaction intermediates were calculated for $N_2O$- and Ar-saturated conditions as a function of NaBr concentration. Such comprehensive information on primary G value allows ones to predict radiation chemical change by considering only homogeneous chemical kinetics.

## Introduction

Water radiolysis has been studied since the discovery of ionizing radiations in the end of the 19th century. [1-3] Ionizing radiations deposit their energies and induce ionizations and excitations of water molecules. Such an ionization leads to production of a highly oxidizing species, water radical cation ($H_2O^{\bullet+}$),[4, 5] and a recoiled electron. $H_2O^{\bullet+}$ becomes a hydroxyl radical ($^{\bullet}OH$) by giving a proton ($H^+$) to one of neighboring water molecules, leading to production of a hydronium cation ($H_3O^+$). On the other hand, the recoiled electron is thermalized and solvated to be a hydrated electron ($e^-_{aq}$). Briefly speaking, water decomposition products after physical and physicochemical stages within 1 ps are mostly $^{\bullet}OH$ and $e^-_{aq}$. These radicals are localized in narrow regions called *"spur"*. Due to such localization as well as their high reactivity, they react with each other in parallel to their diffusions to perimeter region. Such reactions are called as intra-spur reactions and much different from homogeneous chemistry after complete diffusions. As a result of intra-spur reactions, some of $^{\bullet}OH$ and $e^-_{aq}$ are consumed while hydrogen peroxide ($H_2O_2$), molecular hydrogen ($H_2$) and $OH^-$ are produced. Most of the features of radiation-induced chemical reactions are strongly related to spur structure and intra-spur dynamics of radical species.

Pulse radiolysis is a powerful tool to directly observe radiolytic species.[6, 7] The species most widely investigated by the technique is without any doubt $e^-_{aq}$ because it has a strong absorption band in visible and near infrared region with peak around 720 nm. As is noted above, $^{\bullet}OH$ is as much important as $e^-_{aq}$ in water radiolysis, however, few pulse radiolysis studies were conducted to observe it directly. This is because $^{\bullet}OH$ has a very weak absorption band in ultraviolet region with peak around 240 nm. Note that maximum molar absorption coefficient of $e^-_{aq}$ is 19000 $M^{-1}cm^{-1}$ [8] while that of $^{\bullet}OH$ is about 700 $M^{-1}cm^{-1}$. [9] Then, reaction mechanisms and rate constants of $^{\bullet}OH$ have been investigated by utilizing many different scavengers which give rather stable and easily detectable intermediates.

Halide anions such as chloride and bromide anions ($Cl^-$ and $Br^-$) are ones of the most often used $^{\bullet}OH$ scavengers and their radiation chemistry have been intensively discussed.[10-15] Scavenging reactions of halide anions lead to production of rather stable intermediates with strong absorption bands in near ultraviolet or visible region. However, production mechanisms of the intermediates are very complicated and some intermediates have similar absorption bands overlapping with each other. There are several reports on molar absorption coefficients of $BrOH^{\bullet-}$, $Br_2^{\bullet-}$, and $Br_3^-$.[16-20]

Sworski measured yield of production of $H_2O_2$ from aqueous bromide solution with varying $Br^-$ concentration as well as saturating gas.[21] Measured yields were stoichiometrically discussed but detailed reaction dynamics were not able to be considered. Zehavi and Rabani pointed out absorption observed in UV domain in aqueous bromide

solutions would be attributed to $Br_3^-$.[13] Ershov *et al.* observed formation of $Br_3^-$ in radiation-chemical oxidation of $Br^-$ in an aqueous solution by pulse radiolysis, showing optical characteristics of $Br_3^-$ and its equilibrium, $Br_2 + Br^- \leftrightarrow Br_3^-$.[22] It would be worth noting that optical absorption bands and equilibrium constants of trihalide anions such as $Br_3^-$, $Br_2Cl^-$, $BrCl_2^-$, and $Cl_3^-$ were well investigated without any ionizing radiation by Wang *et al.*[23] LaVerne *et al.* investigated on production of $H_2$ in the radiolysis of aqueous bromide solutions.[24] They concluded that oxidizing species containing bromide atom are recycled in the reaction with reducing species such as $e^-_{aq}$, $H^•$, and $HO_2^•$ although detailed mechanism including rate constants were not well clarified. Lin *et al.* scrutinized spectral change of $Br^-$, $Br_2^{•-}$, and $Br_3^-$ as a function of temperature and pressure from ambient to supercritical condition with nanosecond pulse radiolysis technique although detailed mechanism of sequential radiation chemical reactions in bromide solution was not well clarified.[25] Thus, most of discussions in the past reports are based on yields of final products after irradiations.

It is clear that sequential radiation chemical reactions in aqueous bromide solutions begin from the scavenging reaction toward $^•OH$, leading to production of a stable product, $Br_3^-$. Due to high stability of $Br_3^-$, it was proposed to utilize $Br_3^-$ production in concentrated bromide solutions in chemical dosimetry.[26] Direct effect onto solutes, $Br^-$, becomes non-negligible with increasing its concentration and was discussed with picosecond pulse radiolysis technique and final product analysis after $^{60}$Co γ-irradiation.[14, 27, 28] Increase of bromide concentration not only make direct effect non-negligible but also affects competition among the sequential radiation chemical reactions. In order to precisely predict the change of competition, it is necessary to strictly separate contribution of each reaction composing the sequence. Bromide anion has been widely used not only as a probe of $^•OH$ but also as an inhibitor of $H_2O_2$ production via the reaction between two $^•OH$ radicals as well as of $H_2$ destruction via the reaction between $H_2$ and $^•OH$.[29-34] Furthermore, $Br^-$ has been used in radiation chemistry not only of low LET (linear energy transfer) radiations such as fast electrons and γ-rays but also of high LET radiations such as ion beams. Ion beam pulse radiolysis studies with aqueous bromide solutions were performed to investigate yield and behavior of $^•OH$ in heavy ion tracks.[35, 36] Primary yields of $^•OH$ for several therapeutic high-energy heavy ions were estimated from difference in $H_2O_2$ productions from aerated aqueous solutions containing $Br^-$ and formate anions ($HCOO^-$).[37, 38] Thus, influence of $Br^-$ in the sequential reactions in water radiolysis is of crucial importance. In this study, it was purposed to resolve contribution of each reaction by electron pulse radiolysis experiments as well as by spur diffusion model simulations. Based on the simulations, which are validated by reproducing all of the experimental results, variation of primary G values of major water decomposition products as well as major reaction intermediates involving Br atom are reported. Note that primary G value is yield after sufficient diffusions during 100 ns, which allows ones to predict radiation chemical effect by considering only homogeneous chemical kinetics.

## Pulse Radiolysis Experiment

Pulse radiolysis experiments were carried out with an electron beam provided from a linear accelerator, LINAC, at Nuclear Professional School, the University of Tokyo. Energy and pulse width of the beam were 35 MeV and 10 ns, respectively. Other details of the system are described elsewhere.[39] Each sample solution was gradually flown through a quartz cell with 20-mm optical path to avoid interference by accumulated stable products. Dosimetry was done with the thiocyanate dosimeter,[40] which is an $N_2O$-saturated aqueous solution of 10 mM KSCN. The highest dose per single pulse was 47.0 Gy. An aluminum plate of a few millimeter thickness was located at the end of the accelerator to reduce dose given to sample down to 14.3 Gy.

All sample preparations were done with ultrapure water (> 18.3 MΩ cm) from a Milli-Q system (Merck KGaA). Sodium bromide (NaBr, > 99.9%), sodium perchlorate ($NaClO_4$, > 98%), sodium hydroxide (NaOH, > 95.0%), and potassium thiocyanate (KSCN, > 99.5%) were purchased from Wako Pure Chemical Industries, Ltd. and used without any further purification. Concentrations of aqueous bromide solutions were 0.9, 9, 90 and 900 mM, which were bubbled with $N_2O$ or Ar gas for 30 minutes or longer just before irradiation. It would be worth noting that $e^-_{aq}$ is converted into $^•OH$ by $N_2O$ gas as follows:[13, 41]

$$e^-_{aq} + N_2O \rightarrow O^{•-} + N_2 \qquad 9.1\times10^9\ M^{-1}s^{-1}$$
$$O^{•-} + H_2O \rightarrow {}^•OH + OH^- \qquad 9.4\times10^7\ M^{-1}s^{-1}$$

The reaction time scales of the first and second steps are 4.4 and 0.19 ns, respectively, because of concentration of water itself, 55.6 M, and solubility of $N_2O$ into water, 25 mM.

## Spur Diffusion Model Simulation

Radiolytic products such as $^•OH$ and $e^-_{aq}$ are initially localized in spur. To mimic spur processes, it is necessary to take into account not only chemical reactions but also diffusions due to concentration gradients. Spur diffusion model is a simple deterministic model but a powerful tool to explain intra-spur behaviors of water radiolysis products.[42, 43] Generally, initial distributions of water decomposition products at the beginning of the simulation, i.e. 1 ps after irradiation, are given by 3D symmetric Gaussian distributions. The model requires solving simultaneous differential equations of multiple variables. FACSIMILE for Windows version 4.2 (MCPA Software Ltd.) is a software for numerical calculations and was used to solve the differential equations. Details of the concrete methodology are summarized in our previous report.[44] Input parameters for the simulation were slightly modified to reproduce the latest report of fast behaviors of water decomposition radicals within a few nanoseconds.[45, 46] Standard deviation of the Gaussian distribution for $e^-_{aq}$ and that for the other species were modified to 3.20 and 1.15 nm, respectively. A reaction set for radioysis of pure water was taken from AECL report 2009.[47] Other reactions related to bromide ions were taken from a report of Kelm and Bohnert.[15] Diffusion coefficients used for $Br^-$, $Br^•$, $Br_2^{•-}$, $BrOH^{•-}$, $Br_3^-$ and $Br_2$ are 2.1, 2.1, 1.2, 1.1, 1.1, and $1.1\times10^{-5}$ $cm^2/s$, respectively, which are the same as those used in a literature.[34]

It is well known that dose rate can affect behaviors of radiolytic species. Such a dose rate effect is explained by overlapping of neighboring spurs.[48] In the present simulations, spherical space was considered with a boundary condition that all chemical species cannot go out from the sphere or come in from its outside. In short, the size of the sphere is corresponding to the half of averaged distance between neighboring spurs. Assuming that all spurs appear simultaneously and their intervals are all equal to twice of the



 

radius of the sphere, $r_0$ m, there must be the following relationship.

$$\frac{4\pi}{3} r_0^{\ 3} = \frac{E}{\rho X}$$

where, $\rho$ is the density of the aqueous solution (~ 0.001 kg/m$^3$), $E$ is the average energy necessary to produce a single spur ($10^{-17}$ J (= 62.5 eV)), $X$ is the dose per pulse in the unit of gray (J/kg). Specifically, the radii ($r_0$) corresponding to dose of 47.0 and 14.3 Gy are 37.0 and 55.1 nm, respectively.

High concentration of salt can affect solubility of gas in solution, which is called as *"salting out/in"*. The solubility of $N_2O$ gas into water is interfered by high concentration of NaBr. Schumpe proposed a universal function,[49] from which the following relationship is derived in the case of pH 7.

$$[N_2O] = [N_2O]_0 \exp\left(-0.1308 C_{NaBr} - 7.56\times10^{-9}\right)$$
$$\approx 0.8774^{C_{NaBr}} [N_2O]_0$$

where, $[N_2O]_0$ is concentration without any salt (25 mM), $C_{NaBr}$ is dissolved concentration of NaBr in the unit of molar. Based on the function, concentrations of dissolved $N_2O$ in aqueous solutions of 0.9, 9, 90 and 900 mM NaBr are estimated as 25, 25, 24 and 20 mM, respectively.

Rate constants of reactions between charged species are affected by ionic strength. In short, increasing ionic strength accelerates reactions between charged species of a same sign and decelerates those between charged species of opposite signs. The ionic strength effect was taken into account by following established models.[50, 51]

## Results and discussion

### Absorption Spectra of $BrOH^{\bullet-}$ and $Br_2^{\bullet-}$

Figure 1 shows normalized absorption spectra observed with an $N_2O$ saturated 0.9 mM NaBr aqueous solution. Both of the spectra commonly have peaks around 360 nm, however, their shapes are slightly different and the spectrum becomes narrower with time. The experimentally observed spectra at 100 and 500 ns agree very well with reported spectra of $BrOH^{\bullet-}$ and $Br_2^{\bullet-}$,[18] respectively, shown as solid lines. Thus, $BrOH^{\bullet-}$ appears as a reaction intermediate within 100 ns, and then, is gradually converted into $Br_2^{\bullet-}$ during the time range from 100 to 500 ns.

Fig. 2 shows a scheme of sequential radiation chemical reactions expected to occur in aqueous bromide solutions. As the first step, $^{\bullet}OH$ is scavenged by $Br^-$ to be $BrOH^{\bullet-}$.

$^{\bullet}OH + Br^- \leftrightarrow BrOH^{\bullet-}$ $1.1\times10^{10}$ $M^{-1}s^{-1}$ (forward) (R1)
$3.0\times10^{7}$ $s^{-1}$ (backward)

There are following two pathways for $BrOH^{\bullet-}$ to become $Br_2^{\bullet-}$ depending on $Br^-$ concentration. In the case of rather high $Br^-$ concentration, (R2) is predominant, and $BrOH^{\bullet-}$ reacts directly with $Br^-$ to be $Br_2^{\bullet-}$.

$BrOH^{\bullet-} + Br^- \rightarrow Br_2^{\bullet-} + OH^-$ $1.9\times10^{8}$ $M^{-1}s^{-1}$ (R2)

On the other hand, in the case of rather low $Br^-$ concentration, forward reaction of (R3) is faster than (R2). Thus, $BrOH^{\bullet-}$ dissociates into $OH^-$ and $Br^{\bullet}$, which immediately reacts with $Br^-$ to be $Br_2^{\bullet-}$ (R4).

$BrOH^{\bullet-} \leftrightarrow Br^{\bullet} + OH^-$ $4.2\times10^{6}$ $s^{-1}$ (forward) (R3)
$1.3\times10^{10}$ $M^{-1}s^{-1}$ (backward)

$Br^{\bullet} + Br^- \leftrightarrow Br_2^{\bullet-}$ $1.0\times10^{10}$ $M^{-1}s^{-1}$ (forward) (R4)
$2.5\times10^{4}$ $M^{-1}s^{-1}$ (backward)

The branching ratio between the two pathways is fifty-fifty at the bromide concentration of about 20 mM.

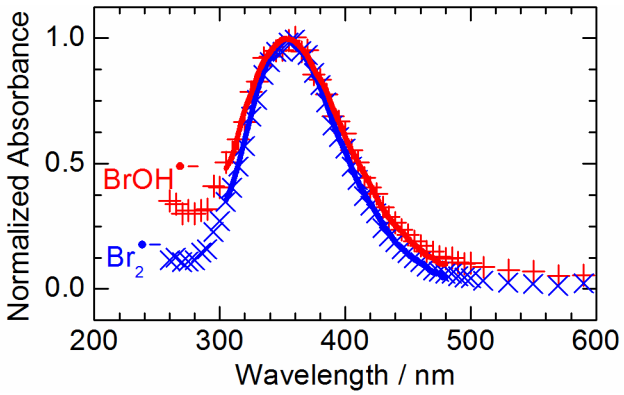


**Fig. 1** Normalized absorption spectra of $BrOH^{\bullet-}$ and $Br_2^{\bullet-}$. (+,×): normalized absorption spectra experimentally observed with an $N_2O$ saturated aqueous solution of 0.9 mM NaBr at 100 and 500 ns after the pulse, respectively, (solid lines): reported spectra of $BrOH^{\bullet-}$ and $Br_2^{\bullet-}$.[18]

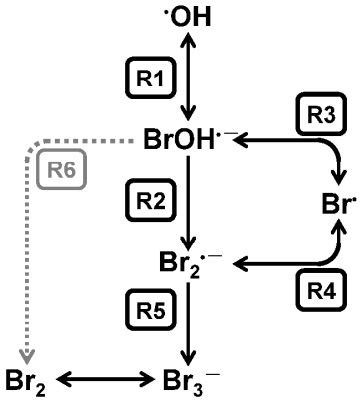


**Fig. 2** A scheme of sequential radiation chemical reactions in aqueous bromide solutions.

**Table 1** Important reactions in aqueous bromide solutions

| Index | Reaction | | | Rate constant / $10^{10}$ $M^{-1}s^{-1}$ | |
|---|---|---|---|---|---|
| R1 | $^{\bullet}OH + Br^-$ | ↔ | $BrOH^{\bullet-}$ | $k_{1f}$ $ | 0.87 (1.1) # |
| | | | | $k_{1b}$ *,$ | 0.003 |
| R2 | $BrOH^{\bullet-} + Br^-$ | → | $Br_2^{\bullet-} + OH^-$ | $k_2$ | 0.019 |
| R3 | $BrOH^{\bullet-}$ | ↔ | $Br^{\bullet} + OH^-$ | $k_{3f}$ *,$ | $4.5\times10^{-4}$ ($4.2\times10^{-4}$)# |
| | | | | $k_{3b}$ $ | 1.3 |
| R4 | $Br^{\bullet} + Br^-$ | ↔ | $Br_2^{\bullet-}$ | $k_{4f}$ $ | 1.0 |
| | | | | $k_{4b}$ *,$ | $2.5\times10^{-6}$ |
| R5 | $Br_2^{\bullet-} + Br_2^{\bullet-}$ | → | $Br_3^- + Br^-$ | $k_5$ | 0.14 (0.34) # |
| R6 | $BrOH^{\bullet-} + BrOH^{\bullet-}$ | → | products | $k_6$ | 0.38 (0) # |

* Unit for first order reactions such as $k_{1b}$, $k_{3f}$ and $k_{4b}$ is $s^{-1}$. $ The subscripts indicate directions of the reactions (f: forward, b: backward). # The rate constants in the table are the values re-estimated in this work and some of them are slightly different from the values reported by Kelm and Bohnert,[15] which are written in parentheses.

After that, $Br_2^{\bullet-}$ decays through a disproportionation reaction to produce $Br_{3-}$.

$Br_2^{\bullet-} + Br_2^{\bullet-} \rightarrow Br_3^- + Br^-$ $1.4\times10^9$ $M^{-1}s^{-1}$ (R5)

One of the products, $Br_3^-$, is in an equilibrium, $Br_2 + Br^- \leftrightarrow Br_3^-$, of which equilibrium constant is 17.4 $M^{-1}$.[22] In this paper, the equilibrium was not taken into account because mostly we focused on experimental data obtained at 360 nm, where only $BrOH^{\bullet-}$ and $Br_2^{\bullet-}$ have strong absorptions. Note that the rate constants of the reactions (R1)-(R5) were taken from a report[8] and are slightly different from the values optimized in this work (see table 1 below).

### Molar Absorption Coefficient and Decay Kinetics of $Br_2^{\bullet-}$

The bottom panel of Fig. 3 shows temporal behaviors of absorbance at 360 nm observed with $N_2O$ saturated aqueous bromide solutions of 0.9, 9, and 900 mM. The peak value of the absorbance increased with $Br^-$ concentration, showing that $^{\bullet}OH$ scavenging by $Br^-$ (R1) becomes predominant in competition with $^{\bullet}OH$ consumption in spur reactions. The build-up behavior within 5 μs or less depends on $Br^-$ concentration, which is reasonable because reaction rates of (R2) and (R4) are proportional to $Br^-$ concentration.

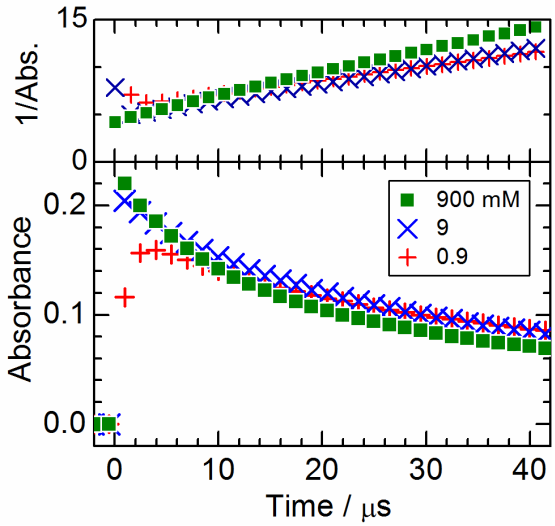


**Fig. 3** Build-up and decay kinetics experimentally observed at 360 nm. (+, ×, ■): $N_2O$ saturated aqueous solutions of 0.9, 9 and 900 mM, respectively. Note that the upper panel shows reciprocal plots of the data in the lower panel.

In the upper panel of the figure, reciprocal plots of the temporal behaviors are shown. They are all on straight lines except for build-up within 5 μs or less, implying that the decays are due to the disproportionation reaction of $Br_2^{\bullet-}$ (R5). Slope of the straight line gives $2k_{app}/\varepsilon\ell$ for each condition, where $\varepsilon$, $\ell$, and $k_{app}$ are molar absorption coefficient of $Br_2^{\bullet-}$ at 360 nm, optical path (2 cm), and apparent rate constant of (R5) at a given ionic strength condition. The value of $\varepsilon$ is necessary when estimating the value of $k_{app}$ from the slope. Several values have been reported for $\varepsilon$ as follows; 9600±800[17], 7800±2000[19], 8200[20], and 9900±600 $M^{-1}cm^{-1}$.[52] One of the reasons for the dispersion is difficulty in separating absorption of $Br_2^{\bullet-}$ from $BrOH^{\bullet-}$ because the two species have very similar absorption bands. Recently, Lampre *et al.* carefully separated the bands of the two species by a pulse radiolysis system combined with a streak camera as well as by a Bayesian data analysis.[18] They concluded molar absorption coefficients of $Br_2^{\bullet-}$ and $BrOH^{\bullet-}$ are 9600±300 and 7800±300 $M^{-1}cm^{-1}$ at their peak positions of 354 and 352 nm, respectively. In the present study, molar absorption coefficients at 360 nm were estimated from the ratio of absorbance at 360 nm to that at the peak wavelength (9500 for $Br_2^{\bullet-}$ and 7700 $M^{-1}cm^{-1}$ for $BrOH^{\bullet-}$). Employing 9500 $M^{-1}cm^{-1}$ as $\varepsilon$, the value of $k_{app}$ for $Br^-$ concentrations of 0.9, 9, 90, and 900 mM were determined as 1.48, 1.74, 2.04 and $2.53\times10^9$ $M^{-1}s^{-1}$, respectively. The dependence of the apparent rate constant on ionic strength agrees well with the established models,[50, 51] which allowed ones to re-evaluate rate constant at the limit of ionic strength of zero, $k_{5f}$, as $1.4\times10^9$ $M^{-1}s^{-1}$. The re-evaluate value is smaller than a reported value[15] by a factor of 2.4 although this difference would be due to lack of correction of the ionic strength effect in the past works.

### Optimization of Rate Constants

Spur diffusion model simulations were conducted with the re-evaluated rate constant, $k_{5f}$. Fig. 4 shows time profile of absorbance experimentally observed at 360 nm in an $N_2O$-saturated 0.9 mM NaBr aqueous solution in comparison to simulation results. Experimental result shown as open circles comprises fast build-up within 100 ns and rather slow build-up after that. The sequential reactions proceed in the order of (R1), (R3) and (R4) (see Fig. 2) at this $Br^-$ concentration, so the flexion point at 100 ns is due to conversion from $BrOH^{\bullet-}$ to $Br_2^{\bullet-}$ via $Br^{\bullet}$. The dotted line in the figure shows a simulation result with rate constants of the reactions (R1)-(R4) reported by Kelm and Bohnert[15] (see table 1). The simulation result clearly overestimates the experimental result. It was attempted to vary molar absorption coefficients of $BrOH^{\bullet-}$ and $Br_2^{\bullet-}$ within the range of the latest report,[18] however, the difference couldn't be resolved. Thus, it was necessary to carefully re-examine the rate constants in the simulation.

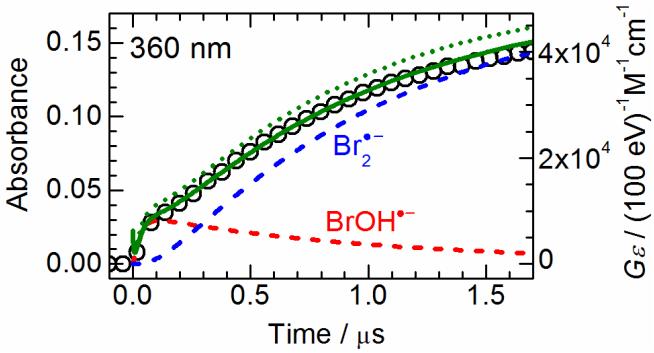


**Fig. 4** Time-dependent absorbance observed with an $N_2O$-saturated aqueous solution containing 0.9 mM sodium bromide in comparison to simulations. (○): experimental result observed at 360 nm, (dotted and solid lines): simulation results before and after modification of rate constants ($k_{1f}$ and $k_{3f}$), respectively, (dashed lines): contributions of $BrOH^{\bullet-}$ and $Br_2^{\bullet-}$ in the simulation after consideration of (R6). For simulation results, see the vertical axis on the right.

Among the four reactions (R1)-(R4), rate constant of (R4) is reported by several groups and the values agree with each other, i.e. $k_{4f} = (1.0\pm0.3)\times10^{10}$ $M^{-1}s^{-1}$. On the other hand, rate constants of the reactions (R1)-(R3) are reported in only one publication[6] and might be less reliable. Then, these rate constants were optimized to reproduce the experimental result. Concretely speaking, $k_{1f}$ and $k_{3f}$ were modified from 1.1 to $0.87\times10^{10}$ $M^{-1}s^{-1}$ and from 4.2 to $4.5\times10^6$ $s^{-1}$, respectively.

Contributions of $BrOH^{\bullet-}$ and $Br_2^{\bullet-}$ after the optimization are shown as dashed lines, and their summation is shown as solid line, which agrees well with the experimental result.

### Disproportionation Reaction of $BrOH^{\bullet-}$

The same experiments were done for other conditions of $Br^-$ concentrations of 0.9, 9, 90 and 900 mM as well as Ar-saturation. Obtained experimental results at 360 nm are shown in figure 5 in the form of $G\varepsilon$, which was calculated from observed absorbance and dose by the following relation.

$$G\varepsilon = \frac{100eN_A}{\rho\ell}\frac{Abs.}{X} \approx 4.82\times10^6\frac{Abs.}{X}$$

where, $N_A$ is the Avogadro's number ($6.022\times10^{23}$ $mol^{-1}$), and *Abs.* is absorbance. Spur diffusion model simulations conducted with the optimized rate constants could not well reproduce the experimental results at high concentrations, i.e. 90 and 900 mM (data are not shown). The $G\varepsilon$ values at 1 μs and later obtained by the simulations increased with increasing $Br^-$ concentration while those in experiments were not much different for $Br^-$ concentration range from 9 to 900 mM. Such a discrepancy was consistently seen in both $N_2O$- and Ar-saturated conditions. Increasing scavenger concentration corresponds to acceleration of scavenging time scale. In the present study, increasing $Br^-$ concentration from 9 to 900 mM corresponds to acceleration of scavenging time scale for $^{\bullet}OH$ from 10 to 0.1 ns. It is known that $^{\bullet}OH$ decays from 5.2 $(100\ eV)^{-1}$ at 1 ps to 2.8 $(100\ eV)^{-1}$ at 100 ns in pure water due to intra-spur reactions as follows.

$^{\bullet}OH + {}^{\bullet}OH \rightarrow H_2O_2$ $\quad 4.8\times10^9\ M^{-1}s^{-1}$

$^{\bullet}OH + e^-_{aq} \rightarrow OH^-$ $\quad 3.5\times10^{10}\ M^{-1}s^{-1}$

Thus, scavenged amounts of $^{\bullet}OH$ in 9 and 900 mM bromide solutions must be different although produced amount of $Br_2^{\bullet-}$ are comparable for the $Br^-$ concentrations. Only one possibility that can call off this discrepancy is that there is a not yet reported reaction, through which some of scavenged $^{\bullet}OH$ is lost before production of $Br_2^{\bullet-}$.

As is explained above, $^{\bullet}OH$ and $e^-_{aq}$ are initially localized in spur, and their distributions become homogeneous after diffusions and intra-spur reactions during 100 ns. As far as scavenging reaction occurs within 100 ns, reaction intermediates such as $BrOH^{\bullet-}$, $Br^{\bullet}$, and $Br_2^{\bullet-}$ appear inside the spur. Averaged diffusion distance of $^{\bullet}OH$, $x$ m, at time, $t$ s, is given by the following equation,

$$x = \sqrt{6Dt}$$

where, $D$ is diffusion coefficient of $^{\bullet}OH$ ($2.3\times10^9$ $m^2/s$). The averaged diffusion distance of $^{\bullet}OH$ before scavenging reaction (R1) decreases from 37 to 1.2 nm with increasing $Br^-$ concentration from 0.9 to 900 mM. Therefore, the time and space where $BrOH^{\bullet-}$ and $Br_2^{\bullet-}$ appear becomes faster and narrower, respectively, with increasing $Br^-$ concentration. Due to the localization of the intermediates, the reactions among $^{\bullet}OH$, $BrOH^{\bullet-}$, $Br^{\bullet}$, and $Br_2^{\bullet-}$ would be non-negligible especially for high $Br^-$ concentration conditions. Among these reactions, there are reports on rate constants of $^{\bullet}OH + {}^{\bullet}OH \rightarrow H_2O_2$ and $Br_2^{\bullet-} + Br_2^{\bullet} \leftrightarrow Br_3^- + Br^-$, which were already incorporated in the simulations. In addition, $Br^{\bullet}$ hardly exists in high $Br^-$ concentration conditions. Thus, the following four reactions might be candidates of *"a not yet reported reaction"*.

$BrOH^{\bullet-} + BrOH^{\bullet-} \rightarrow Br_2 + 2OH^-$ (R6)

$BrOH^{\bullet-} + Br_2^{\bullet-} \rightarrow$ products

$BrOH^{\bullet-} + {}^{\bullet}OH \rightarrow$ products

$Br_2^{\bullet-} + {}^{\bullet}OH \rightarrow Br_2 + OH^-$

Among the candidates, only the reaction $BrOH^{\bullet-} + BrOH^{\bullet-}$ (R6) was effective and non-negligible. Spur diffusion model simulations were re-conducted with consideration of (R6), rate constant of which was optimized as $3.8\times10^9\ M^{-1}s^{-1}$. It is worth noting that a reaction similarly to (R6), $COO^{\bullet-} + {}^{\bullet}OH \rightarrow$ products, is reported in a study using aqueous solutions containing concentrated formate.[53] Results of the simulations are shown as solid lines in Fig. 5. Note that contribution of direct effects was taken into account for all of the simulation results shown in the figure. In short, simulation results without consideration of direct effects were multiplied by a factor of the ratio of numbers of electrons in whole solution to that in solvent, which are 1.0001, 1.0007, 1.0075 and 1.0745 for 0.9, 9, 90 and 900 mM NaBr aqueous solutions, respectively. More accurately, direct effects in the system are ionizations of $Br^-$ and $Na^+$, giving $Br^{\bullet}$, $Na^{2+}$ and $e^-_{aq}$. $Na^{2+}$ might be able to be produced but it would soon remove one electron from neighboring water molecules, giving $H_2O^{\bullet+}$ or $^{\bullet}OH$. In addition, $Br^{\bullet}$ soon reacts with $Br^-$ to be $Br_2^{\bullet-}$ in high concentration of $Br^-$, reaction time scale of which is 0.1 ns for 1 M $Br^-$. It is clearly seen that the simulations agree very well with the experimental results for a wide variety of conditions such as saturating gas and $Br^-$ concentration. Reactions of $e^-_{aq}$ are important in Ar-saturated conditions.

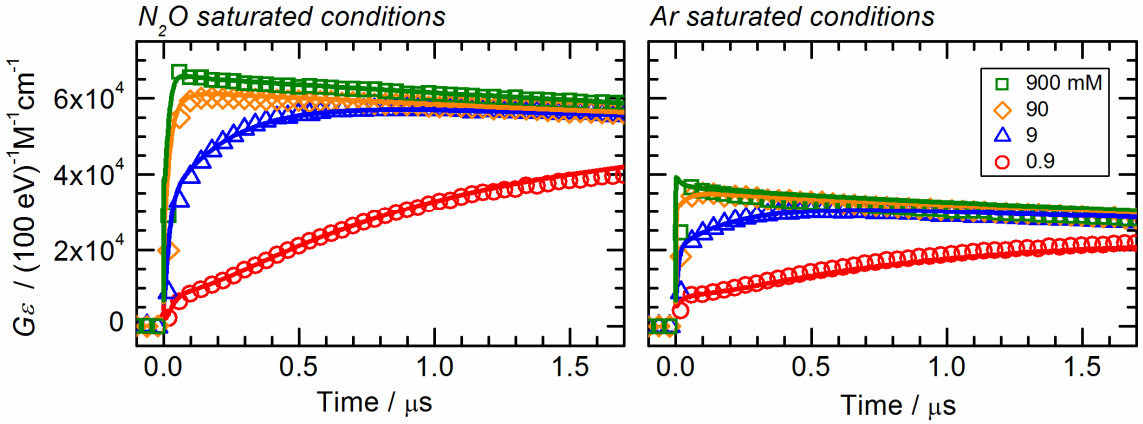


**Fig. 5** Comparison between experiments and simulations with the revised rate constants. Left and right panels show data of $N_2O$- and Ar-saturated conditions, respectively. (○, △, ◇, □): experimental results for aqueous solutions of 0.9, 9, 90 and 900 mM NaBr, respectively, (solid lines): simulation results for corresponding conditions. Note that contribution of direct effects was taken into account in all of the simulation results shown in this figure.

The decay seen in Ar-saturated conditions were not only due to the disproportionation reaction of $Br_2^{\bullet-}$ (R6) but also due to the following reaction.[51]

$e^-_{aq} + Br_2^{\bullet-} \rightarrow 2Br^- \qquad 1.1\times10^{10}\ M^{-1}s^{-1}$

In addition, $e^-_{aq}$ is not converted into $^{\bullet}OH$ at Ar-saturated conditions, so contribution of $e^-_{aq}$ was taken into account with molar absorption coefficient of 1535 $M^{-1}cm^{-1}$, which is obtained by extrapolating a function reported by Bartels *et al.*[8] Increasing concentration of metal cation leads to blue shift of absorption band of $e^-_{aq}$ due to, *so-called*, contact pair structure.[14, 54, 55] Molar absorption coefficient of $e^-_{aq}$ at 360 nm might be slightly higher than the value used in the present work due to the blue shift. Based on the fact that absorption band width does not change within the blue shift,[56, 57] molar absorption coefficient of $e^-_{aq}$ at 360 nm in 1 M NaBr aqueous solution would be same as that at 361-364 nm in neat water, which is 1550-1590 $M^{-1}cm^{-1}$. Thus, possible increase of contribution of $e^-_{aq}$ in this study is at most 1%-4%.

Direct observation of the reaction (R6) was attempted, however, it was quite difficult due to the following two reasons. First, as is claimed above, absorption band of $BrOH^{\bullet-}$ mostly overlaps with that of $Br_2^{\bullet-}$. Second, experimental condition to keep $BrOH^{\bullet-}$ alive for sufficiently long duration is very limited because it tends to be converted into $Br^{\bullet}$ or $Br_2^{\bullet-}$. As seen in Fig. 2, $BrOH^{\bullet-}$ dissociates into $Br^{\bullet}$ with reaction time scale of 200 ns (forward reaction of (R3)) or reacts with $Br^-$ to be $Br_2^{\bullet-}$ with reaction time scale between 6 ns and 6 μs (R2), depending on $Br^-$ concentration. Of course, there is a backward reaction of (R3), and its reaction time scale depends on pH; ca. 1 ms at pH 7 and ca. 100 ns at pH 11. Thus, condition is limited to $Br^-$ concentration lower than 30 mM as well as pH higher than 11, in order to observe $BrOH^{\bullet-}$ for 100 ns. In addition, dissociation of $^{\bullet}OH$ into $O^{\bullet-}$ at high pH also restricts experimental conditions. Possible products in the reaction (R6) would be $Br_2$ and $OH^-$ or $H_2O_2$ and $Br^-$. It was confirmed that there is no obvious increase of $H_2O_2$ with increasing $Br^-$ concentration, implying that the most probable products are $Br_2$ and $OH^-$. Due to the equilibrium between $Br_2$ and $Br_3^-$, yield of $Br_3^-$ after sufficient time is stoichiometrically not affected by (R6) at conditions of high $Br^-$ concentration. Note that all simulations with (R6) were conducted with assuming these products.

### Primary Yields of Reaction Intermediates

Temporal behaviors of water decomposition radicals and reaction intermediates within the sequential reactions are shown in Fig. 6. Solid and dotted lines are simulation results with and without (R6), respectively. It is clear that (R6) is effective in the cases of $Br^-$ concentration of 90 and 900 mM, however, production yield of $Br_3^-$ at the end of the simulation, 1 ms, is not affected by (R6). This is because $Br_2$ is assumed as a product of (R6), which immediately becomes $Br_3^-$ via a reaction with $Br^-$ at high $Br^-$ concentrations. Decay of $^{\bullet}OH$ as well as build-up of $BrOH^{\bullet-}$ corresponds to progress of (R1). Note that $Br_3^-$ production via (R6) occurs within 1 μs while it is much slower than that via the other pathways. Decay of $BrOH^{\bullet-}$ as well as build-up of $Br_2^{\bullet-}$ corresponds to progress of (R2) except the case of the lowest $Br^-$ concentration. $Br^{\bullet}$ appears only at the lowest concentration (0.9 mM) because (R3) followed by (R4) is predominant in conversion from $BrOH^{\bullet-}$ into $Br_2^{\bullet-}$ while (R2) is predominant in the other cases. Note that an increase of $^{\bullet}OH$ yield from 1 to 100 ns for 0.9 mM $Br^-$ is conversion from $e^-_{aq}$.

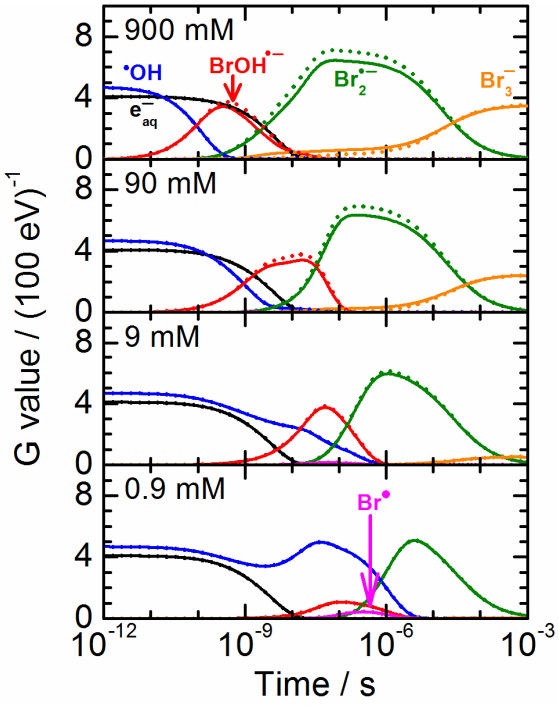


**Fig. 6** Simulated temporal behaviors of major products in $N_2O$-saturated aqueous bromide solutions. (Dotted and solid lines): G values of transient species with and without the consideration of (R6), respectively. Note that all data shown in the figure are without correction of direct effect contribution.

Balcerzyk *et al.* measured yield of a final product, $Br_3^-$, at various conditions.[27] For example, the yield of $Br_3^-$ in an $N_2O$-saturated condition of 2 M NaBr aqueous solution is reported as 4.13 $(100\ eV)^{-1}$. Similarly to the present work, they conducted spur diffusion model simulations, showing that they could reproduce the $Br_3^-$ yield, which was also able to be reproduced by our simulations. The largest difference between simulations of the two studies is seen in decay of $Br_2^{\bullet-}$ and build-up of $Br_3^-$. They intensively worked on picosecond pulse radiolysis as well,[14, 28] however, behaviors of reaction intermediates in medium time scale were not observed in their experiments.

Primary G values, which are yields after sufficient diffusions for a hundred nanoseconds, are of crucial importance because such information allows ones to predict radiation chemical effect by considering only homogeneous chemical kinetics. Fig. 7 shows primary G values of important reaction intermediates as a function of $Br^-$ concentration. Increase of $Br^-$ concentration accelerates the forward reaction of (R1), leading to decrease of primary G value of $^{\bullet}OH$. Corresponding to the trend, primary G value of $BrOH^{\bullet-}$ increases but begins to decrease at $Br^-$ concentration of approximately 10 mM. Beyond the concentration, primary G value of $Br_2^{\bullet-}$ increases, which are due to acceleration of (R2). In addition, primary G value of $Br_3^-$ becomes non-negligible for higher $Br^-$ concentrations, resulted from faster rate constant of (R5) due to the ionic strength effect as well as from larger primary yield of $Br_2^{\bullet-}$. Primary yield of $H_2O_2$ decreases with increasing $Br^-$ concentration. This is because $^{\bullet}OH$ is converted into $BrOH^{\bullet-}$ or $Br_2^{\bullet-}$ before the reaction, $^{\bullet}OH + {}^{\bullet}OH \rightarrow H_2O_2$, proceeds. It is worth noting that such a trend of $H_2O_2$ yield as a function of $Br^-$ concentration was, recently, carefully discussed by Mustaree *et al.* [34]

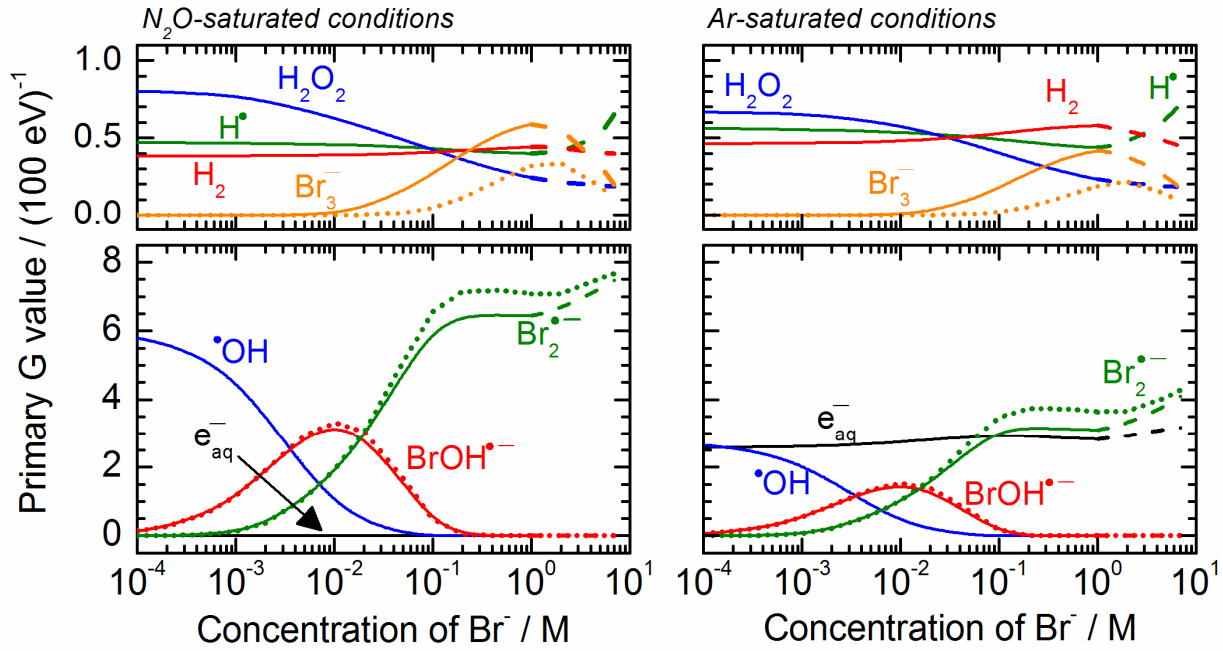


**Fig. 7** Primary G values of transient species appearing in aqueous bromide solutions as a function of bromide concentration. All data in the figure are simulation results and not corrected in terms of direct effects. Left and right panels are for $N_2O$- and Ar-saturated conditions, respectively. In order to avoid too much complexity, products with rather low and high primary yields are separately shown in upper and bottom panels, respectively. Note that the results for concentration of 1 M and higher are shown as dashed lines because direct effects are non-negligible in the bromide concentration range. Dotted lines show results without consideration of (R6).

It is seen that primary G values of $H^•$ and $Br_2^{•-}$ slightly increase in the $Br^-$ concentration higher than 1 M. This tendency is explained as follows. In the models of Czapski and Schwarz[50] and D'Angelantonio *et al.*[51], the ionic strength effect is moderated as opposed to the trend below 1 M. As a result, the reaction, $e^-_{aq} + H^+ \rightarrow H^•$, is accelerated, and the reaction, $Br_2^{•-} + Br_2^{•-} \rightarrow Br_3^- + Br^-$ (R5) is decelerated. Note that direct effect was not taken into account here. Of course, direct effect becomes more and more significant in concentrated solutions. In addition, a strong oxidizing species produced by ionization of water molecule, $H_2O^{•+}$,[4, 5] can react with $Br^-$ to be $H_2O$ and $Br^•$, followed by (R4) and leading to instant production of $Br_2^{•-}$. This pathway becomes non-negligible in concentrated solutions[14, 27, 28] and should be taken into account in further accurate discussion in higher $Br^-$ concentrations.

## Conclusions

Electron pulse radiolysis experiments with time resolution of 10 ns and spur diffusion model simulations were performed to resolve contributions of each reaction in aqueous bromide solutions of a wide variety of conditions. Reaction rate constant of the disproportionation reaction of $Br_2^{•-}$, $Br_2^{•-} + Br_2^{•-} \rightarrow Br_3^- + Br^-$, at the limit of ionic strength of zero was evaluated as $1.4\times10^9$ $M^{-1}s^{-1}$, which is slightly smaller than reported values ($1.6\text{-}3.4\times10^9$ $M^{-1}s^{-1}$). A not yet reported reaction, $BrOH^{•-} + BrOH^{•-} \rightarrow Br_2 + 2OH^-$, was necessary to be introduced into the simulation with rate constant of $3.8\times10^9$ $M^{-1}s^{-1}$ in order to universally reproduce the experimental results.

Primary G values of major water decomposition products as well as major reaction intermediates involving Br atom were reported as a function of bromide concentration from 0.1 mM to 7 M. Such information is inevitably important when predicting radiation chemistry by considering only homogeneous chemical reactions. Contribution of the introduced reaction was extracted from the simulations, showing that this reaction can be significant for $Br^-$ concentration higher than approximately 10 mM. Yield of a final product, $Br_3^-$, after sufficient duration (> 1 ms) is not much affected by the reaction, however, its production via the reaction occurs within 1 μs while it is much slower via the other pathways. Apparently, the reaction needn't exixt as far as only initial and final states of the sequential reactions are focused on. However, a product of the reaction, $Br_2$, is rather stable, and then, a reaction between $BrOH^{•-}$ and a certain additive would not be as effective as expected without the disproportionation reaction of $BrOH^{•-}$. This point is important in detailed discussion of seawater radiolysis because it contains not only chloride (0.56 M) but also bromide (0.82 mM) and some other components.[58] Oxidizing species in bromide solutions tend to exist in the form of $BrOH^{•-}$ in the equilibrium, $Br^- + {}^•OH \leftrightarrow BrOH^{•-}$, however, those in chloride solutions tend to be free $^•OH$ in a similar equilibrium, $Cl^- + {}^•OH \leftrightarrow ClOH^{•-}$. Such a difference leads to difference in $H_2$ productions in bromide and chloride solutions. $H_2$ production in Ar-saturated 1 mM $Br^-$ solution increases linearly at least up to 100 kGy while there is almost no $H_2$ production in 1 mM $Cl^-$ solution.[24] Even with a small amount of $Br^-$ compared to $Cl^-$, the former is more predominant in $H_2O_2$ production, which is one of the most responsible oxidizing species in oxidative corrosion.[59, 60] Another notable point is that $^•OH$ is produced in ion tracks with very high local concentration, which would lead to high local concentration of $BrOH^{•-}$ as well. In that case, the disproportionation reaction of $BrOH^{•-}$ would be non-negligible even if bromide concentration is not so high.

## Acknowledgements

We are grateful to Mr. T. Ueda and Prof. M. Uesaka (Univ. Tokyo) for their technical assistance and encouragement in pulse radiolysis experiments.

## Notes and references

[a] Nuclear Professional School, School of Engineering, the University of Tokyo, 2-22 Shirakata-shirane, Tokai-mura, Naka-gun, Ibaraki 319-1188, Japan.

[b] Department of Nuclear Engineering and Management, School of Engineering, the University of Tokyo, 7-3-1 Hongo, Bunkyo-ku, Tokyo 113-8656, Japan.

[c] Quantum Beam Science Center, Japan Atomic Energy Agency, 1233 Watanuki-machi, Takasaki, Gunma 370-1292, Japan.

[d] Nuclear Safety Research Center, Japan Atomic Energy Agency, 2-4 Shirakata-shirane, Tokai-mura, Naka-gun, Ibaraki 319-1195, Japan.

[e] Department of Beam Materials Science, Institute of Scientific and Industrial Research, Osaka University, 8-1 Mihogaoka, Ibaraki, Osaka 567-0047, Japan.

1. A. O. Allen, *The Radiation Chemistry of Water and Aqueous Solutions*, Van Nostrand, New York, 1961.
2. G. V. Buxton, in *Charged Particle and Photon Interactions with Matter. Chemical, Physicochemical, and Biological Consequences with Applications*, eds. A. Mozumder and Y. Hatano, Marcel Dekker, New York, 2004, pp. 331-363.
3. I. G. Draganić and Z. D. Draganić, *The Radiation Chemistry of Water*, Academic Press, New York and London, 1971.
4. J. Ma, U. Schmidhammer, P. Pernot and M. Mostafavi, *J. Phys. Chem. Lett.*, 2014, **5**, 258-261.
5. J. Ma, U. Schmidhammer and M. Mostafavi, *J. Phys. Chem. A*, 2014, **118**, 4030-4037.
6. J. Belloni, R. A. Crowell, Y. Katsumura, M. Lin, J. L. Marignier, M. Mostafavi, Y. Muroya, A. Saeki, S. Tagawa, Y. Yoshida, V. De Waele and J. F. Wishart, in *Recent Trends in Radiation Chemistry*, eds. J. F. Wishart and B. S. M. Rao, World Scientific Publishing, Singapore, 2010, pp. 121-160.
7. E. Janata, in *Recent Trends in Radiation Chemistry*, eds. J. F. Wishart and B. S. M. Rao, World Scientific Publishing, Singapore, 2010, pp. 97-120.
8. D. M. Bartels, K. Takahashi, J. A. Cline, T. W. Marin and C. D. Jonah, *J. Phys. Chem. A*, 2005, **109**, 1299-1307.
9. M. S. Alam and E. Janata, *Chemical Physics Letters*, 2006, **417**, 363-366.
10. M. Kelm, V. Metz, E. Bohnert, E. Janata and C. Bube, *Radiat. Phys. Chem.*, 2011, **80**, 426-434.
11. A. Mamou, J. Rabani and D. Behar, *J. Phys. Chem.*, 1977, **81**, 1447-1448.
12. S. Sunder and H. Christensen, *Nucl. Technol.*, 1993, **104**, 403-417.
13. D. Zehavi and J. Rabani, *J. Phys. Chem.*, 1972, **76**, 312-319.
14. A. K. El Omar, U. Schmidhammer, A. Balcerzyk, J. A. LaVerne and M. Mostafavi, *J. Phys. Chem. A*, 2013, **117**, 2287-2293.
15. M. Kelm and E. Bohnert, *A Kinetic Model for the Radiolysis of Chloride Brine, its Sensitivity against Model Parameters and a Comparison with Experiments* FZKA 6977, Institut für Nuleare Entsorgung, Karlsruhe, 2004.
16. B. Čerček, *Int. J. Radiat. Phys. Chem.*, 1972, **4**, 25-30.
17. B. Čerček, M. Ebert, A. J. Swallow and J. P. Keene, *Science*, 1964, **145**, 919-920.
18. I. Lampre, J. L. Marignier, M. Mirdamadi-Esfahani, P. Pernot, P. Archirel and M. Mostafavi, *J. Phys. Chem. A*, 2013, **117**, 877-887.
19. M. S. Matheson, W. A. Mulac, J. L. Weeks and J. Rabani, *J. Phys. Chem.*, 1966, **70**, 2092-2099.
20. H. C. Sutton, G. E. Adams, J. W. Boag and B. D. Michael, in *Pulse Radiolysis*, eds. M. Ebert, J. P. Keene, A. J. Swallow and J. H. Baxendale, Academic Press, New York, 1965, pp. 61-81.
21. T. J. Sworski, *J. Am. Chem. Soc.*, 1954, **76**, 4687-4692.
22. B. G. Ershov, A. V. Gordeev, E. Janata and M. Kelm, *Mendeleev Commun.*, 2001, 149-150.
23. T. X. Wang, M. D. Kelley, J. N. Cooper, R. C. Beckwith and D. W. Margerum, *Inorg. Chem.*, 1994, **33**, 5872-5878.
24. J. A. LaVerne, M. R. Ryan and T. T. Mu, *Radiat. Phys. Chem.*, 2009, **78**, 1148-1152.
25. M. Z. Lin, P. Archirel, N. T. Van-Oanh, Y. Muroya, H. Y. Fu, Y. Yan, R. Nagaishi, Y. Kumagai, Y. Katsumura and M. Mostafavi, *J. Phys. Chem. A*, 2011, **115**, 4241-4247.
26. M. Mirdamadi-Esfahani, I. Lampre, J. L. Marignier, V. de Waele and M. Mostafavi, *Radiat. Phys. Chem.*, 2009, **78**, 106-111.
27. A. Balcerzyk, J. A. LaVerne and M. Mostafavi, *J. Phys. Chem. A*, 2011, **115**, 4326-4333.
28. A. Balcerzyk, U. Schmidhammer, A. K. El Omar, P. Jeunesse, J. P. Larbre and M. Mostafavi, *J. Phys. Chem. A*, 2011, **115**, 9151-9159.
29. A. O. Allen and R. A. Holroyd, *J. Am. Chem. Soc.*, 1955, **77**, 5852-5855.
30. I. Štefanić and J. A. LaVerne, *J. Phys. Chem. A*, 2002, **106**, 447-452.
31. Farhataz., *J. Phys. Chem.*, 1967, **71**, 598-602.
32. M. H. Parajon, R. Raiesh, T. Mu, S. M. Pimblott and J. A. LaVerne, *Radiat. Phys. Chem.*, 2008, **77**, 1203-1207.
33. B. Pastina, J. A. LaVerne and S. M. Pimblott, *J. Phys. Chem. A*, 1999, **103**, 5841-5846.
34. S. Mustaree, J. Meesungnoen, S. L. Butarbutar, P. Causey, C. R. Stuart and J.-P. Jay-Gerin, *RSC Adv.*, 2014, **4**, 43572-43581.
35. G. Baldacchino, G. Vigneron, J. P. Renault, S. Le Caer, S. Pin, J. C. Mialocq, E. Balanzat and S. Bouffard, *Nucl. Instrum. Methods Phys. Res. Sect. B-Beam Interact. Mater. Atoms*, 2006, **245**, 288-291.
36. K. Iwamatsu, M. Taguchi, Y. Sugo, S. Kurashima and Y. Katsumura, *Trans. Mater. Res. Soc. Jpn.*, 2011, **36**, 329-332.
37. S. Yamashita, Y. Katsumura, M. Lin, Y. Muroya, T. Miyazakia and T. Murakami, *Radiat. Phys. Chem.*, 2008, **77**, 439-446.
38. S. Yamashita, Y. Katsumura, M. Z. Lin, Y. Muroya, T. Maeyama and T. Murakami, *Radiat. Phys. Chem.*, 2008, **77**, 1224-1229.
39. K. Hata, M. Z. Lin, Y. Katsumura, Y. Muroya, H. Y. Fu, S. Yamashita and H. Nakagawa, *J. Radiat. Res.*, 2011, **52**, 15-23.
40. G. V. Buxton and C. R. Stuart, *J. Chem. Soc. Faraday Trans.*, 1995, **91**, 279-281.
41. G. V. Buxton, C. L. Greenstock, W. P. Helman and A. B. Ross, *J. Phys. Chem. Ref. Data*, 1988, **17**, 513-886.
42. W. G. Burns, H. E. Sims and J. A. B. Goodall, *Radiat. Phys. Chem.*, 1984, **23**, 143-180.
43. A. Kuppermann, *Diffusion Kinetics in Radiation Chemistry: An Assessment*, Technical, Information Center, Office of Information Services, U.S. Atomic Energy Commission, 1974.



 

44. S. Yamashita, G. Baldacchino, T. Maeyama, M. Taguchi, Y. Muroya, M. Z. Lin, A. Kimura, T. Murakami and Y. Katsumura, *Free Radic. Res.*, 2012, **46**, 861-871.
45. A. K. El Omar, U. Schmidhammer, P. Jeunesse, J. P. Larbre, M. Z. Lin, Y. Muroya, Y. Katsumura, P. Pernot and M. Mostafavi, *J. Phys. Chem. A*, 2011, **115**, 12212-12216.
46. Y. Muroya, M. Z. Lin, G. Z. Wu, H. Iijima, K. Yoshi, T. Ueda, H. Kudo and Y. Katsumura, *Radiat. Phys. Chem.*, 2005, **72**, 169-172.
47. A. J. Elliot and D. M. Bartels, *The Reaction Set, Rate Constants and G-values for the Simulation of the Radiolysis of Light Water over the Range 20°C to 350°C Based on Information Available in 2008* AECL 153-127160-450-001, Atomic Energy of Canada, Ltd., Chalk River, Canada, 2009.
48. D. R. Short, C. N. Trumbore and J. H. Olson, *J. Phys. Chem.*, 1981, **85**, 2328-2335.
49. A. Schumpe, *Chem. Eng. Sci.*, 1993, **48**, 153-158.
50. G. Czapski and H. A. Schwarz, *J. Phys. Chem.*, 1962, **66**, 471-474.
51. M. D'Angelantonio, M. Venturi and Q. G. Mulazzani, *Radiat. Phys. Chem.*, 1988, **32**, 319-324.
52. G. L. Hug, *Optical Spectra of Nonmetallic Inorganic Transient Species in Aqueous Solution* NSRDS-NBS 69, Radiation Chemistry Data Center, Radiation Laboratory, University of Notre Dame, Washington, D.C., 1981.
53. S. Yamashita, Y. Katsumura, M. Z. Lin, Y. Muroya, T. Miyazaki, T. Murakami, J. Meesungnoen and J.-P. Jay-Gerin, *Radiat. Res.*, 2008, **170**, 521-533.
54. J. Bonin, I. Lampre and M. Mostafavi, *Radiat. Phys. Chem.*, 2005, **74**, 288-296.
55. J. Ma, U. Schmidhammer and M. Mostafavi, *J. Phys. Chem. Lett.*, 2014, **5**, 2219-2223.
56. A. N. Asaad, N. Chandrasekhar, A. W. Nashed and P. Krebs, *J. Phys. Chem. A*, 1999, **103**, 6339-6343.
57. J. Bonin, I. Lampre, B. Soroushian and M. Mostafavi, *J. Phys. Chem. A*, 2004, **108**, 6817-6819.
58. Y. Kumagai, A. Kimura, M. Taguchi, R. Nagaishi, I. Yamagishi and T. Kimura, *Journal of Nuclear Science and Technology*, 2013, **50**, 130-138.
59. K. Hata, S. Hanawa, S. Kasahara, Y. Muroya and Y. Katsumura, Nuclear Plant Chemistry Conference 2014 (NPC2014), Sapporo, Hokkaido, Japan, 2014.
60. K. Hata, H. Inoue, T. Kojima, A. Iwase, S. Kasahara, S. Hanawa, F. Ueno and T. Tsukada, *Hydrogen Peroxide Production by Gamma Radiolysis of Concentrated Sodium Chloride Solutions Containing a Small Amount of Bromide Ion*, unpublished work.